Erratum: A_4 lepton flavor model and modulus stabilization from S_4 modular symmetry [Phys. Rev. D 100, 115045 (2019)]

Tatsuo Kobayashi, Yusuke Shimizu, Kenta Takagi, Morimitsu Tanimoto, and Takuya H. Tatsuishi

(Received 6 February 2020; accepted 7 February 2020; published 26 February 2020)

DOI: 10.1103/PhysRevD.101.039904

Equation (24) is incorrect. The correct equation is presented as follows:

$$M_\nu = \frac{\langle H_u \rangle^2}{\Lambda'} \left[\begin{pmatrix} 2Y_3 & -Y_5 & -Y_4 \\ -Y_5 & 2Y_4 & -Y_3 \\ -Y_4 & -Y_3 & 2Y_5 \end{pmatrix} + aY_1 \begin{pmatrix} 0 & 1 & 0 \\ 1 & 0 & 0 \\ 0 & 0 & 1 \end{pmatrix} + bY_2 \begin{pmatrix} 0 & 0 & 1 \\ 0 & 1 & 0 \\ 1 & 0 & 0 \end{pmatrix} \right]. \tag{24}$$

Accordingly, Fig. 1 is replaced in Sec. III, and Figs. 5–10 are replaced in Sec. IV. The numerical results of Sec. V are revised. The conclusion is not changed.

V. PHENOMENOLOGICAL ASPECTS OF LEPTONS

A. Region A

Let us present numerical results for the modulus τ in the region A. The parameter ρ, which realizes the potential minimum for the superpotential (34), is shown in the Re$[\rho]$-Im$[\rho]$ plane in Fig. 5, while Fig. 8 shows ρ' for the potential minimum for the superpotential (35). In this case, only the NH of neutrino masses is available.

First, we show a correlation between δ_{CP} and $\sin^2\theta_{23}$ in Fig. 11. The predicted ranges of δ_{CP} are $[-160°, -140°]$ for $\sin^2\theta_{23} \leq 0.57$ and $[-140°, -135°]$, $[40°, 45°]$ for $\sin^2\theta_{23} \geq 0.57$. We present the predicted δ_{CP} versus the sum of neutrino masses $\sum m_i$ in Fig. 12, where the cosmological bound $\sum m_i < 120$ [meV] is imposed. The predicted δ_{CP} clearly depends on the sum of neutrino masses. For $\sum m_i = [78, 88]$ [meV], δ_{CP} is predicted to be in the range $[-160°, -135°]$. Near the cosmological bound, $\sum m_i = [115, 120]$ [meV], δ_{CP} is $[40°, 45°]$.

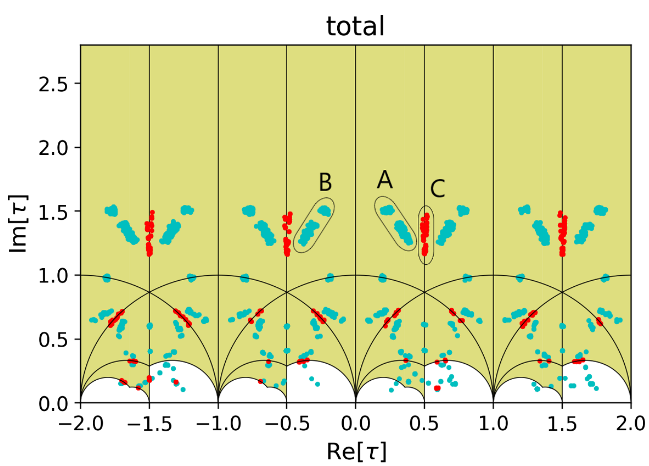

FIG. 1. Allowed regions of τ in the Re$[\tau]$-Im$[\tau]$ plane. The fundamental domain of $\Gamma(4)$ is shaded olive green. Cyan and red points denote the cases of NH and IH, respectively.

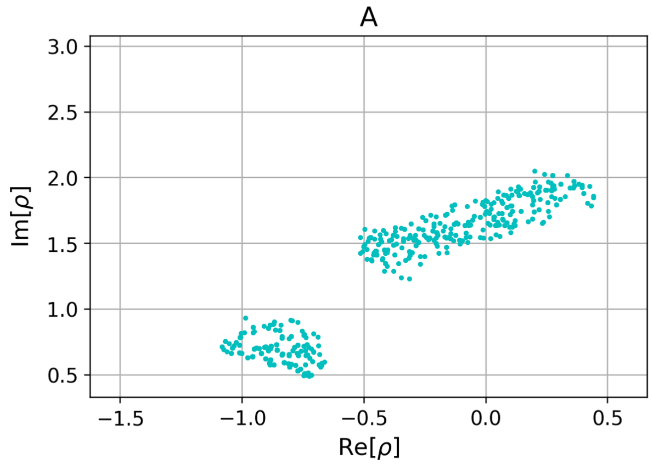

FIG. 5. Values of ρ corresponding to τ in the A region for W in Eq. (34).

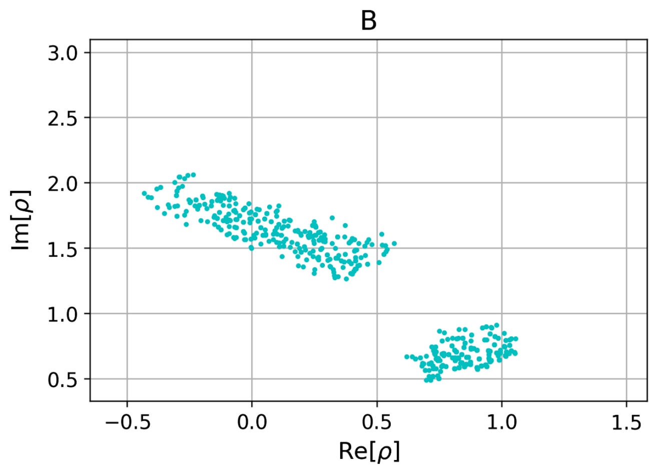

FIG. 6. Values of ρ corresponding to τ in the B region for W in Eq. (34).

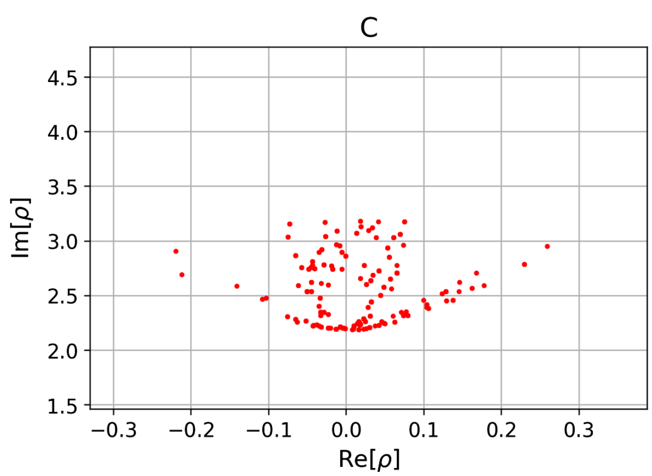

FIG. 7. Values of ρ corresponding to τ in the C region W in Eq. (34).

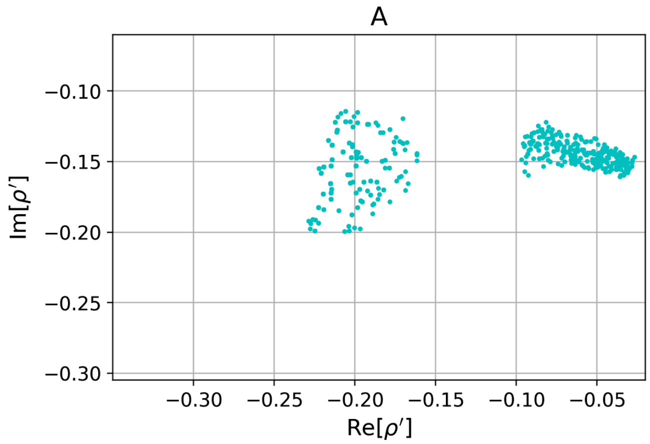

FIG. 8. Values of ρ' corresponding to τ in the A region for W in Eq. (35).

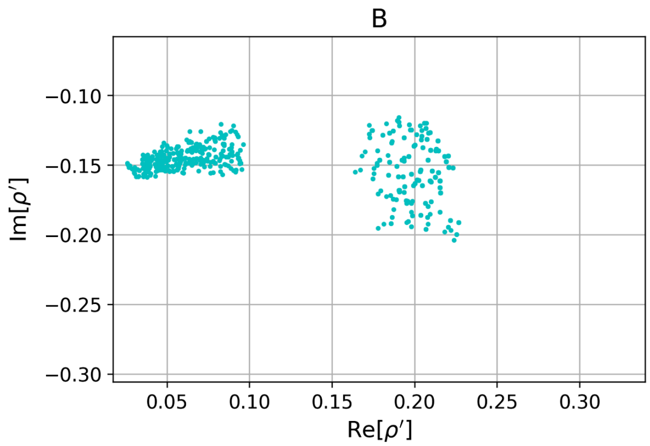

FIG. 9. Values of ρ' corresponding to τ in the B region for W in Eq. (35).

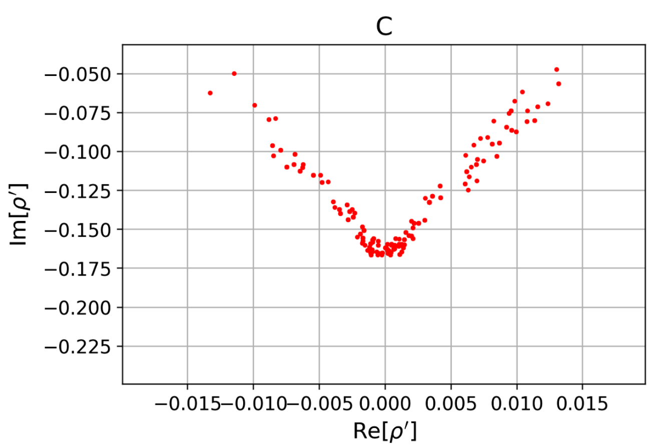

FIG. 10. Values of ρ' corresponding to τ in the C region W in Eq. (35).

On the other hand, there is no clear neutrino mass dependence for $\sin^2\theta_{23}$, as seen in Fig. 13. Near the upper bound of $\sum m_i = 120$ [meV], θ_{23} is predicted in the second octant. The effective mass of the $0\nu\beta\beta$ decay $\langle m_{ee}\rangle$ is presented in Fig. 14. The prediction is in the ranges 9.4–12 and 22–24 [meV]. We summarize the predictions for $\langle m_{ee}\rangle$ and $\sum m_i$ in Table II.

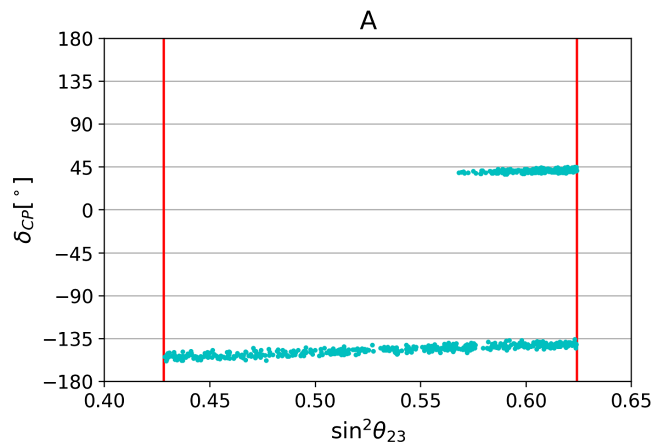

FIG. 11. The predicted region in the $\sin^2\theta_{23}$-δ_{CP} plane in region A for NH. Vertical red lines denote the 3σ bound of observed data.

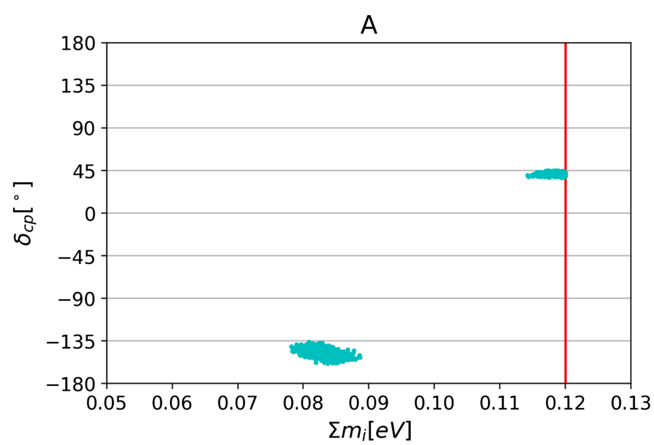

FIG. 12. The sum of neutrino masses $\sum m_i$ dependence of δ_{CP} in region A for NH. The vertical red line denotes the cosmological bound.

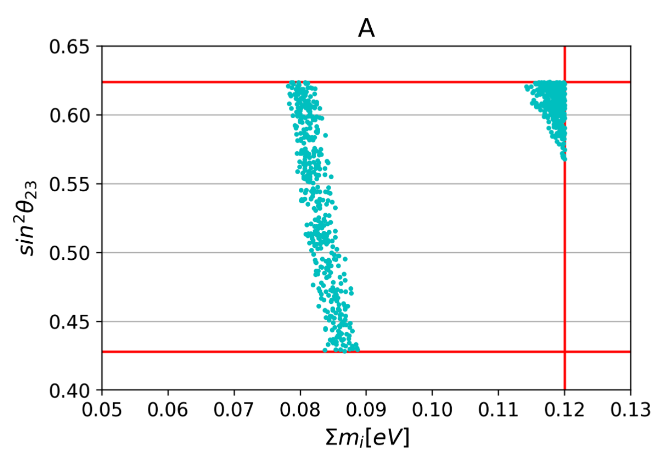

FIG. 13. The sum of neutrino masses $\sum m_i$ dependence of $\sin^2\theta_{23}$ in region A for NH.

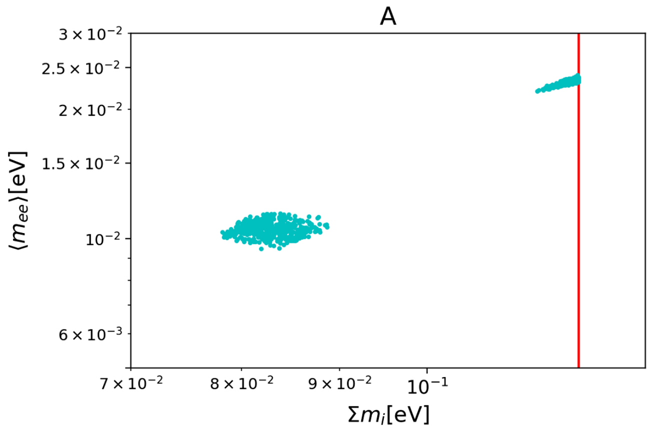

FIG. 14. The predicted effective neutrino mass $\langle m_{ee}\rangle$ versus $\sum m_i$ in region A for NH.

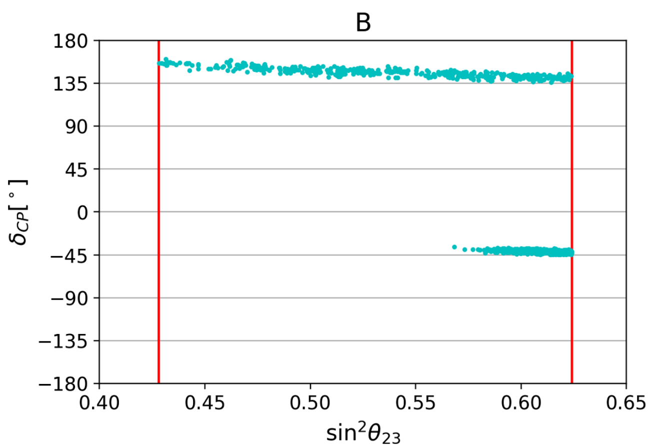

FIG. 15. The predicted region in the $\sin^2\theta_{23}$-δ_{CP} plane in region B for NH. Vertical red lines denote the 3σ bound of observed data.

B. Region B

We discuss the numerical results for the modulus τ in the region B. The parameter ρ, which realizes the potential minimum for the superpotential (34), is shown in the Re[ρ]-Im[ρ] plane in Fig. 6, while Fig. 9 shows ρ' for the potential minimum for the superpotential (35). In this case, only the NH of neutrino masses is available.

We show the correlation between δ_{CP} and $\sin^2\theta_{23}$ in Fig. 15. The predicted ranges of δ_{CP} are [140°,160°] for $\sin^2\theta_{23} \leq 0.57$ and [135°,140°], $[-45°, -40°]$ for $\sin^2\theta_{23} \geq 0.57$. We present the predicted δ_{CP} versus the sum of neutrino masses $\sum m_i$ in Fig. 16. For $\sum m_i = [78, 88]$ [meV], δ_{CP} is predicted to be in the range [135°,160°]. Near the cosmological bound, $\sum m_i = [115, 120]$ [meV], δ_{CP} is $[-45°, -40°]$.

The neutrino mass dependence for $\sin^2\theta_{23}$ is almost the same as the result for region A, as seen in Fig. 17. The effective mass of the $0\nu\beta\beta$ decay $\langle m_{ee}\rangle$ is also the same as the result for region A, as seen in Fig. 18. We summarize the predictions for $\langle m_{ee}\rangle$ and $\sum m_i$ in Table II.

TABLE II. Predicted $\langle m_{ee}\rangle$ and $\sum m_i$ for cases A, B, and C.

	A		B		C	
	NH	IH	NH	IH	NH	IH
$\langle m_{ee}\rangle$ [meV]	9–12, 22–24	×	9–12, 22–24	×	×	15–30
$\sum m_i$ [meV]	77–88, 115–120	×	77–88, 115–120	×	×	98–110

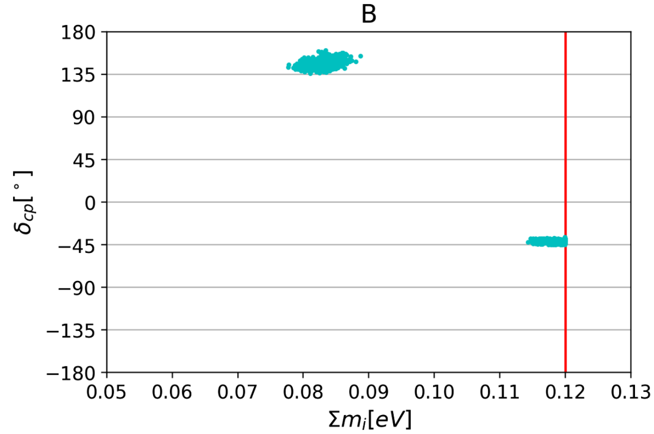

FIG. 16. The sum of neutrino masses $\sum m_i$ dependence of δ_{CP} in region B for NH. The vertical red line denotes the cosmological bound.

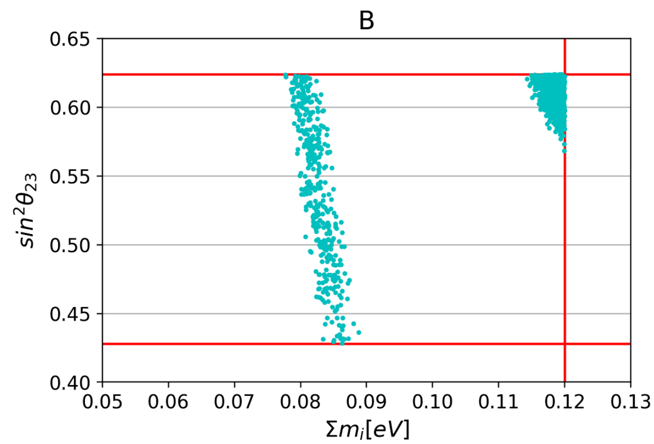

FIG. 17. The sum of neutrino masses $\sum m_i$ dependence of $\sin^2\theta_{23}$ in region B for NH.

C. Region C

Finally, discuss the numerical results for the modulus τ in the region C. The parameter ρ, which realizes the potential minimum for the superpotential (34), is shown in the Re[ρ]-Im[ρ] plane in Fig. 6, while Fig. 9 shows ρ' for the potential minimum for the superpotential (35). In this case, only the IH of neutrino masses is available.

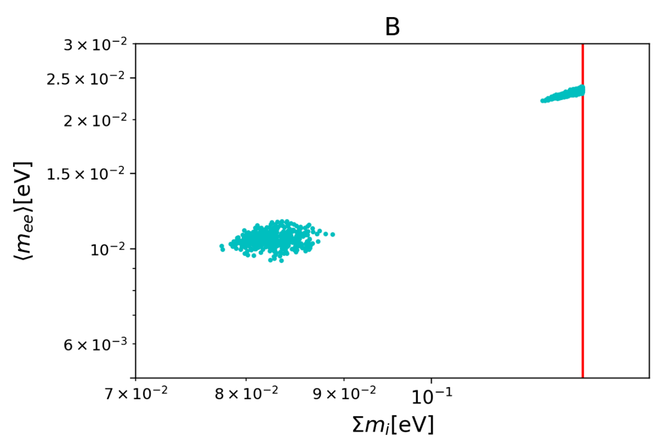

FIG. 18. The predicted effective neutrino mass $\langle m_{ee}\rangle$ versus $\sum m_i$ in region B for NH.

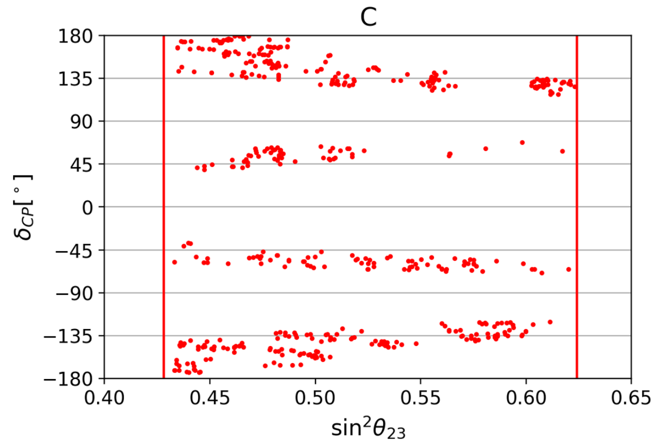

FIG. 19. The predicted region in the $\sin^2\theta_{23}$-δ_{CP} plane in region C for IH. Vertical red lines denote the 3σ bound of observed data.

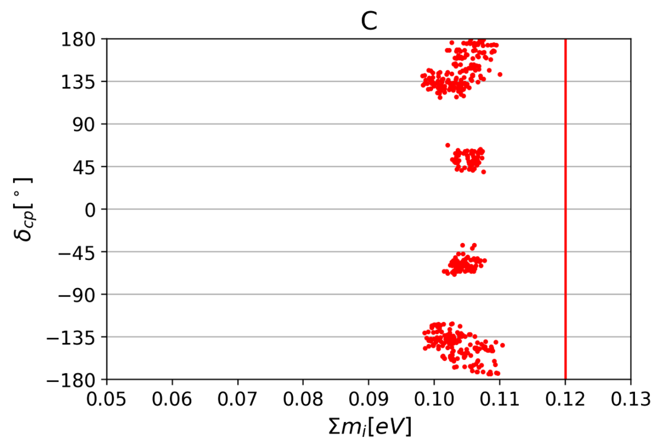

FIG. 20. The sum of neutrino masses $\sum m_i$ dependence of δ_{CP} in region C for IH. The vertical red line denotes the cosmological bound.

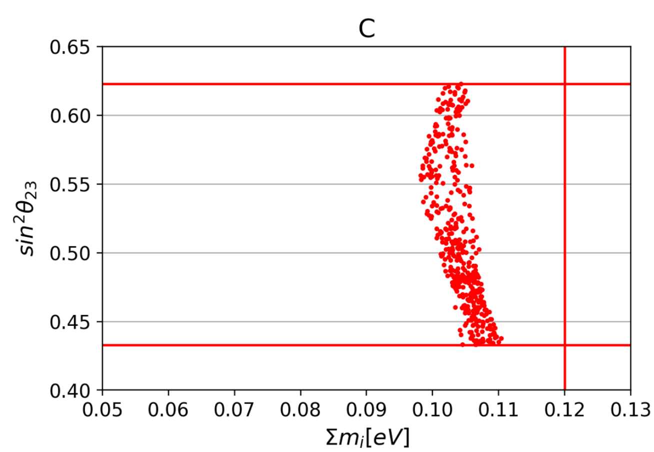

FIG. 21. The sum of neutrino masses $\sum m_i$ dependence of $\sin^2\theta_{23}$ in region C for IH.

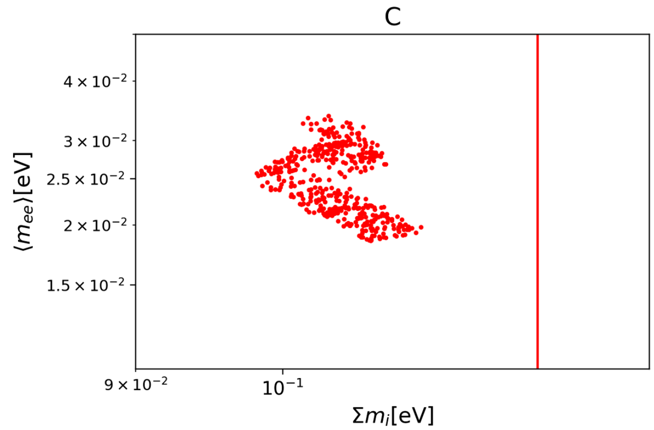

FIG. 22. The predicted effective neutrino mass $\langle m_{ee}\rangle$ versus $\sum m_i$ in region C for IH.

We show the correlation between δ_{CP} and $\sin^2\theta_{23}$ in Fig. 19. We can see the weak $\sin^2\theta_{23}$ dependence for δ_{CP}. The predicted δ_{CP} is in the ranges $\pm[40°, 60°]$ and $\pm[120°, 180°]$. We show the predicted δ_{CP} versus the sum of neutrino masses in Fig. 20. The sum of neutrino masses $\sum m_i$ is restricted to the narrow range $\sum m_i = [98, 110]$ [meV].

There is no clear neutrino mass dependence for $\sin^2\theta_{23}$, as seen in Fig. 21. Below $\sum m_i = 102$ [meV], θ_{23} is predicted in the second octant, while it is in the first octant for $\sum m_i \geq 107$ [meV]. The effective mass of the $0\nu\beta\beta$ decay $\langle m_{ee}\rangle$ is presented in Fig. 22. The prediction is in the range of 18–34 [meV]. We summarize the predictions for $\langle m_{ee}\rangle$ and $\sum m_i$ in Table II.